STAFF SUMMARY SHEET

	TO	ACTION	SIGNATURE (Surname), GRADE AND DATE		TO	ACTION	SIGNATURE (Surname), GRADE AND DATE
1	DFEM	Coord	O-6 23May13	6			
2	DFER	Approve	25 May13	7			
3	DFEM/ CAStLE	Action		8			
4				9			
5				10			

SURNAME OF ACTION OFFICER AND GRADE	SYMBOL	PHONE	TYPIST'S INITIALS	SUSPENSE DATE
Dr. James Greer	HQ USAFA/DFEM	DSN 333-3618	lgm	20130531

SUBJECT		DATE
Review and Release of Research	USAFA-DF-PA- 355	20130521

SUMMARY

1. PURPOSE: To provide security and policy review on the document at Tab 1 prior to release to the public.

2. BACKGROUND:
- Author(s): J.T. Burns, Center for Aircraft Structural Life Extension

- Title: Effect of Water Vapor Pressure on the Fatigue Crack Propagation of Aerospace Aluminum Alloys 7075-T651 and 2199-T86

- Circle One: Abstract Tech Report Journal Article Speech (Paper) Presentation Poster

Thesis Dissertation Book Other:_____

Check all that apply (For Communications Purposes):
[] CRADA (Cooperative Research and Development Agreement) exists
[] Photo/ Video Opportunities [] STEM-outreach Related [] New Invention/ Discovery/ Patent

- Description: Abstract is being submitted to the DoD Corrosion Conference.

- Previous clearance information: USAFA-DF-PA-248 (Abstract)

- Recommended distribution statement: Distribution A, Approved for public release, distribution unlimited.

3. DISCUSSION: This research was performed under the sponsorship of the DoD Office for Corrosion Policy and Oversight under the auspices of their Technical Corrosion Collaboration.

4. RECCOMMEDATION: Department Head or designee review as subject matter expert. DFER review for policy and security and provide public release clearance.

JAMES M. GREER, JR., PhD, PE
Technical Director, CAStLE

1 Tab
1. Conference Paper

EFFECT OF WATER VAPOR PRESSURE ON THE FATIGUE CRACK PROPAGATION OF AEROSPACE ALUMINUM ALLOYS 7075-T651 AND 2199-T86

J.T. Burns
University of Virginia
395 McCormick Dr.
Charlottesville, VA 22904
jtb5r@virginia.edu

ABSTRACT

Fatigue testing over a wide range of ΔK-values, extending into the threshold regime, at various water vapor pressures (P_{H2O}) applicable to airframe operation yielded a novel set of fatigue crack growth rates for two aerospace aluminum alloys (7075-T651 and 2199-T86). Data were analyzed with respect to prominent environmental fatigue theories and used to inform a next generation prognosis aimed at incorporating the effects of loading environment. AA 2199-T86 exhibited enhanced fatigue crack growth rate resistance compared with AA 7075-T651 over a wide range of environmental exposures and ΔK. The da/dN-ΔK data for both alloys shows the expected decrease in crack growth rate with decreasing exposure parameter (P_{H2O}/f). Plotting the growth rate data versus P_{H2O}/f demonstrates consistency with prominent environmental theories where the crack growth is limited by either molecular flow or H-diffusion in the crack tip process zone. In both alloys, ΔK-shed data at intermediate-low exposures shows an apparent threshold followed by an increase in growth rates with falling ΔK. Speculatively, this is due to development of crack wake roughness that initially impeeds molecular flow, increasing roughness then causes convective mixing which enhances flow and increases growth rates. A protocol to select environment appropriate crack growth rates for linear elastic fracture mechanics (LEFM) modeling is presented.

Keywords: fatigue, hydrogen embrittlement, fracture mechanics, prognosis

INTRODUCTION

Next generation fracture mechanics-based prognosis modeling of airframe fatigue damage can increase accuracy (and reduce over-conservatism) by coupling the substantial progress in understanding and modeling mechanical loading spectra with similar efforts to capture the strong influence of an environmental spectrum [2]. Such modeling requires: (1) development of a coupled mechanical (stress, stress intensity range (ΔK), frequency (f)) and environmental spectrum (temperature, water vapor pressure (P_{H2O}), time of wetness, inhibitor concentration) that is representative of airframe component operational conditions. Such a spectrum would be akin to the generic mechanical loading spectra for fighter wings (FALSTAFF), transport lower wing root (TWIST), and helicopter rotors (Helix) [5]. (2) Quantitative characterization of environment specific fatigue crack growth properties for use in linear elastic fracture mechanics (LEFM) prognosis models (e.g. AFGROW, FASTRAN, etc.). (3) Development of an understanding of the governing mechanisms to inform a life prediction methodology that captures the environmental effect without a prohibitive experimental burden. Significant airframe loading occurs at high altitude [6-9] which is typified by low temperature (down to ≈ -70°C) and low water vapor pressure environments [10,11]. Recent work has established that the water vapor pressure over frequency (P_{H2O}/f) exposure parameter does not fully capture the effect of temperature but can be used as a conservative proxy to enable engineering level modeling of the effect of time dependent environmental exposure on fatigue cracking.

Fatigue crack progression is governed by cyclic plastic damage accumulation coupled with grain level local tensile stresses to cause decohesion; H is postulated to enhance this process by facilitating increased dislocation mobility and/or decreasing the local cohesion strength in the crack tip process zone [13-19]. As such the deleterious effect of the loading environment is dependent on the per cycle local concentration of H in the process zone which is set by the loading frequency and the rate limiting step in the H embrittlement process. For aluminum alloys in a moist environment H ingress to the process zone consists of: (a) impeded transport of molecular H_2O from the crack mouth to the crack tip, (b) surface reaction to produce atomic H on the crack tip surface and H absorption, and (c) H diffusion into the crack tip process zone [1, 20, 21]. Models have been proposed that relate da/dN to each of these potential rate limiting steps, despite the change in the controlling process many of these models suggest that crack growth rate is either an explicit or implicit (through setting the atomic H concentration at the crack tip surface) function of P_{H2O}/f [20-26]. These models, and environmental dependence in general, are typically informed by data obtained at constant-high ΔK and variable levels of P_{H2O}/f ; characterization over a wide range of ΔK is generally only performed at isolated exposures and/or does not extend to the near-threshold regime [21,27]. These data enable efficient analysis of the governing mechanisms and model development/validation however are insufficient to fully understand the interaction of ΔK and environmental effects necessary for prognosis efforts. Quantitative crack growth rates over a wide range of ΔK at various exposure levels are necessary inputs to a LEFM-based environmental fatigue life prediction tool; such extensive data-sets will also inform interpolation functions between exposure levels to ease future experimental burdens.

Legacy airframe components rely heavily on 7xxx-series aluminum alloys for structural components. Also of interest are 3rd generation Al-Cu-Li alloys which have remedied the property anisotropy, low toughness, poor corrosion resistance, and manufacturing issues inherent in previous Al-Li alloys [28]. As such the light-weight, high strength/toughness, and enhanced fatigue properties position this alloy class to compete with composites for replacing the incumbent AA 2024 alloys for high stress airframe structural components. Quantification and comparison of the growth rates and fracture morphologies of legacy (7xxx-series) and next generation (3rd generation Al-Cu-Li) aluminum alloys over a wide range of

ΔK and P_{H2O}/f will augment the current understanding of environmental effects in these pertinent aerospace alloys.

The goal of this work is to quantify the crack growth rate (da/dN) behavior of a legacy (AA 7075-T651) and a modern (AA 2199-T86) aerospace alloy over a wide range of mechanical (ΔK) driving forces and exposures (P_{H2O}/f) pertinent to airframe operations. The influence of ΔK on the environmental crack growth behavior will be discussed in the context of the both the H-embrittlement process and a fracture mechanics based life prediction methodology.

EXPERIMENTAL METHODS

Fatigue crack growth rate tests were performed on L-T oriented compact tension (CT) specimens (width 50.8 mm; thickness 7.62 mm) in accordance with ASTM E647, using a computer controlled servo-hydraulic machine to apply a sine waveform. Crack length was calculated from clip gauge measured crack mouth opening displacement using unloading compliance; post-test visual crack length measurements were always within 10% of compliance values and used for data correction. Testing was performed at constant stress ratio (R) of 0.5 and frequency (f) of 20 Hz (with one test at 2 Hz) under a decreasing ΔK protocol (C-value of 0.08 mm^{-1}) from 10 MPa$\sqrt{m}$ to threshold, then an increasing ΔK (C-value of 0.2 mm^{-1}) segment from ≈8 MPa$\sqrt{m}$ to 16 MPa$\sqrt{m}$. Testing was performed at 2668, 340, 165, 38, 4, 0.54 and $5x10^{-7}$ (UHV) Pa; which corresponds with the equilibrium water vapor pressures above water or ice at roughly 23°C (relative humidity of 95%), -7°C, -15°C, -30°C, -50°C, and -65°C, respectively, according to the Clausium-Clapeyron equation (note that UHV does not have a temperature equivalent). The 2688 Pa environment was maintained within a sealed plexiglass cell fed with water saturated nitrogen while the temperature and humidity was continuously monitored to ensure >95% humidity. The remaining tests were performed in an ultra-high vacuum system where varying levels of purified water is introduced through a sealed glass flask via a leak valve; the pressure was dynamically maintained by balanced water vapor input and turbo pumping. The water vapor pressure was monitored throughout testing and a mass spectrometer confirmed better than 95% (by partial pressure) H_2O purity through all tests (the impurities in the vacuum chamber were a mixture of gaseous CO_2 and N_2).

RESULTS AND DISCUSSION

Alloy Comparison at High Humidity and UHV

The superior fatigue performance of Al-Cu-Li alloys compared to traditional Al-Zn-Mg-Cu (and Al-Cu-Mg) alloys over a range of environmental exposures is well documented [1, 28-30]. This behavior is shown in Figure 1 where elevated growth rates are observed for AA 7075 compared to AA 2199 in both high humidity and UHV testing conditions. This behavior is attributed to the interaction of slip with microstructural features and how the resulting crack morphology influences the local crack tip driving force. The primary strengthening phase in peak- and over-aged 7xxx-series alloys is equilibrium incoherent η-phase (or the semi-coherent meta-stable η'-phase) ($Mg(Zn,Al,Mg)_2$). In alloys with >1.6% Cu the non-shearable incoherent phase promotes dislocation looping and homogeneous slip, which limits slip reversibility and crack path tortuosity. Conversely, the shearable δ'-phase (Al_3Li) (and perhaps T_1-phase (Al_2LiCu)) in Al-Cu-Li alloys enables homogenous reversible planar slip and enhances crack closure via increased roughness associated with highly faceted cracking, crack deflection, and mode II displacements [1,27,30,31]. Such extrinsic toughening mechanisms reduce the local crack tip driving force and are hypothesized to govern the enhanced fatigue performance in the Al-

Cu-Li alloys [30]. The convergence of the UHV data in the near-threshold regime is consistent with prior work that showed highly facetted (rough) slip band cracking (SBC) in AA 7075-T651 at low ΔK and inert environments; this morphology may cause extrinsic toughening similar to that observed in AA 2199-T86 [4,12]. Similarly the convergence of AA 7075 and AA 2199 high humidity growth rates in the near threshold regime is consistent with the transition from the tortuous slip band cracking to relatively flat sub-granular and/or near-{100} cleavage cracking observed in peak-aged AA 2090 alloy (LT) at low ΔK and moist environments [31]. Such features would produce similar levels of extrinsic toughening as the flat transgranular high-index features observed in AA 7075 high humidity testing at low ΔK [32]. Such ΔK dependent behavior coupled with the order of magnitude increase in fatigue resistance in UHV highlights the need to quantify the crack growth behavior over a range of exposures and mechanical driving forces. Future characterization of the fracture surface morphology and analysis of the measured levels of closure are needed to conclusively establish the controlling mechanisms.

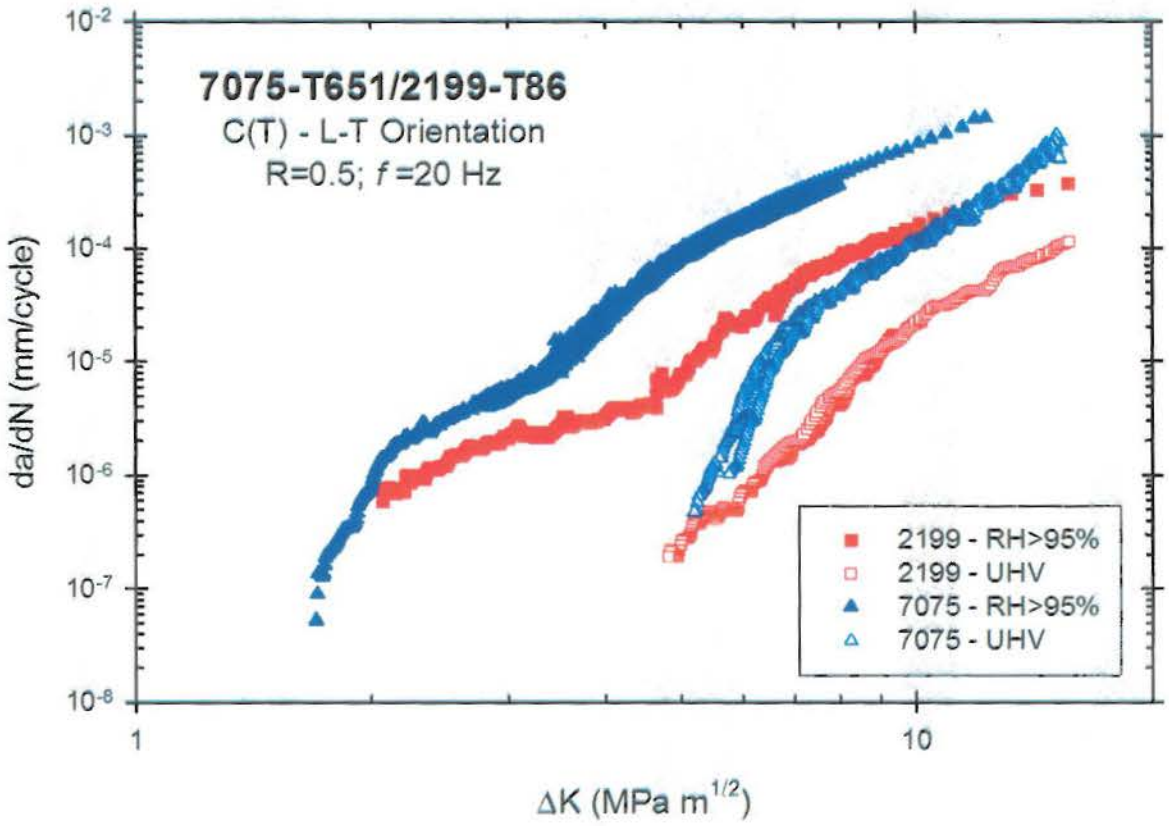

Figure 1: Fatigue crack growth rates vs ΔK for two airframe aluminum alloys tested in a water saturated N_2 environment and at ultra-high vacuum.

7075-T651 Growth Rates at Variable P_{H2O}/f

Fatigue crack growth rates are shown in Figure 2 for AA 7075-T651 as a function of ΔK and the exposure parameter P_{H2O}/f. These growth rates demonstrate the expected decrease in crack growth rate with decreasing water vapor exposure. The similarity in crack growth rates for 1334 (f=2 Hz) and 134 (20 Hz) Pa-s demonstrate that at this exposure the crack growth rate is independent of loading

frequency. Furthermore, the growth rates for 1334 and 133 Pa-s are consistent with the maximum critical growth rate observed for AA 7075-T651 (L-T; R=0.1) tested in 3.5% NaCl, where diffusion controlled crack growth is limited by a mechanics based parameter that governs the maximum increment of growth and is controlled by the location of the maximum tensile stress ahead of the crack tip for a given K_{max} [26]. Decreasing exposure levels from 17 to 1.9 Pa-s corresponds to a reasonably systematic decrease in growth rates at all ΔK. This systematic decrease is also observed for 0.2 and 0.027 Pa-s exposures at ΔK above 6 MPa$\sqrt{m}$ and below 4 MPa$\sqrt{m}$; however, there is a more significant reduction in growth rates between 4 and 6 MPa$\sqrt{m}$ that increases with magnitude going from 0.2 to 0.027 Pa-s. A consistent threshold value of ≈1.8 MPa$\sqrt{m}$ is observed for exposures between 1334 and 0.2 Pa-s, the threshold increased to 2 and 5.3 MPa$\sqrt{m}$ at 0.027 and UHV, respectively.

During the *K*-shed portion of the loading protocol 0.027 Pa-s data show the onset of an apparent

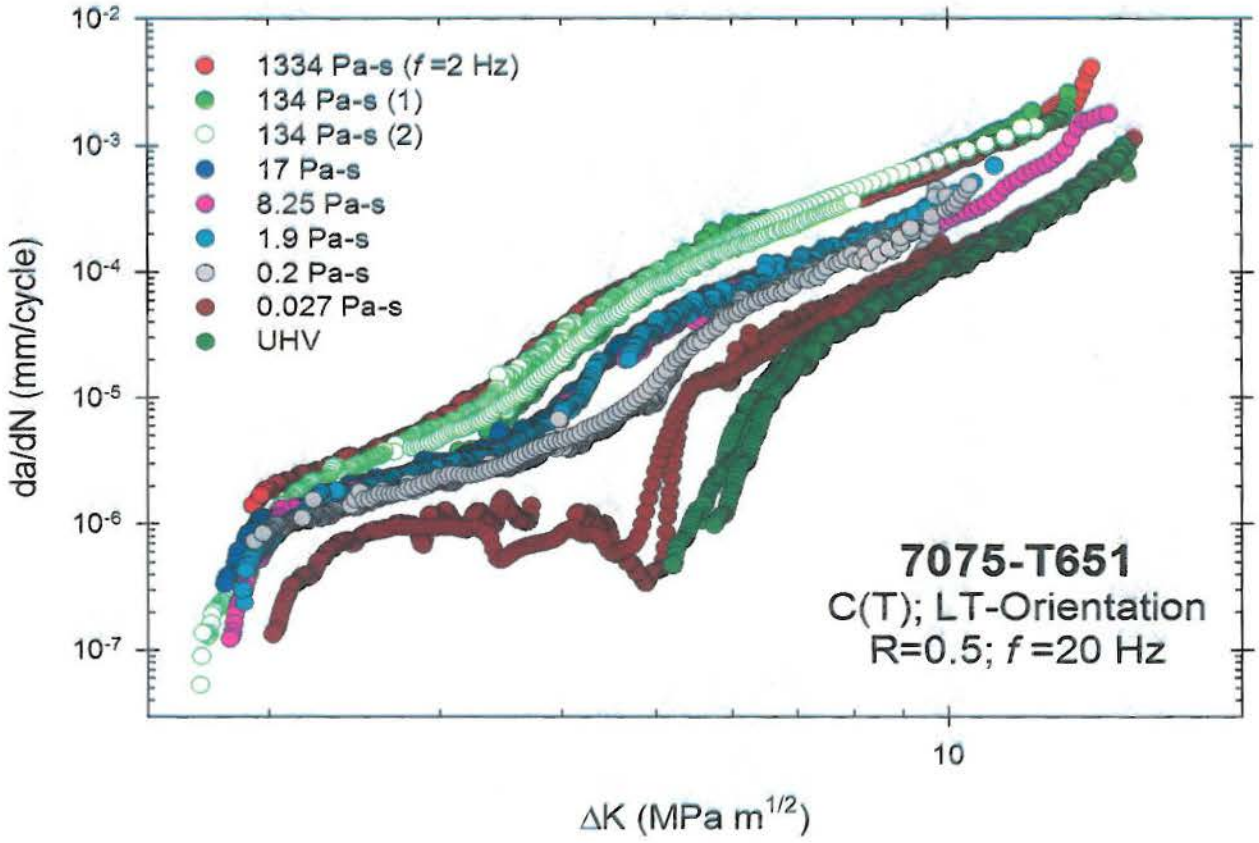

Figure 2: Fatigue crack growth rates vs. ΔK for 7075-T651 tested at R=0.5 in a K-shed and K-rise protocol at various levels of environmental exposure.

threshold at 6 MPa$\sqrt{m}$ that reaches a minima ($3x10^{-7}$ mm/cycle) at 4.9 MPa$\sqrt{m}$, then reverses such that crack growth rate increases as ΔK decreases to 4 MPa$\sqrt{m}$; this is termed the threshold transition. With further reduction below 4 MPa$\sqrt{m}$ the growth rate plateaus before hitting the true threshold at 2 MPa$\sqrt{m}$. During the *K*-rise protocol the growth rate follows a similar plateau up to 4.4 MPa$\sqrt{m}$ and then shows a drastic increase without exhibiting the strong minima seen in the *K*-shed data. The *K*-shed minima is consistent with constant K_{max} (16.5 MPa$\sqrt{m}$)-decreasing ΔK results for this lot of AA 7075-T651 tested in both the L-T and T-L orientations at $3x10^{-4}$, $2.7x10^{-3}$, and $6.5x10^{-3}$ Pa-s at 4 MPa$\sqrt{m}$; where the magnitude of the dip increased with decreasing P_{H2O}/f. A less severe reduction in growth rate was also observed in constant K_{max} data at 0.013 Pa-s similar to the current 0.2 Pa-s results [3]. Fractography of these constant K_{max}-decreasing ΔK specimens showed that the threshold transition behavior directly

correlates with changes in the fracture surface morphology; severe dips exhibited a high density of SBC-like features (high roughness) as compared to a lower density for less severe dips, and no SBC-like features at higher exposures. Fracture surface morphologies not within the dip regions were exclusively flat-transgranular features. The development of SBC-like features are critically dependent on the level of H-enhanced cracking; in inert environments SBC has been observed at low ΔK levels in AA 7075, at high ΔK slip is homogenized across multiple slip systems and SBC features are not observed [12]. The apparent threshold behavior was hypothesized to be due to a reduction in diffusion governed molecular flow (Knudsen flow) caused by the onset of surface roughness development associated with SBC that occurs when the K-shed reaches sufficiently low ΔK [33]. This roughness starves the crack tip of molecular water causing the initial drop in growth rates. However once a critical level/distance of roughness was achieved the dominant means of molecular transport switches from diffusion to convective mixing, which may be fully turbulent due to crack surface contact [34-36]. Such mixing would provide enhanced water vapor transport, thus cauing the increase in growth rate.

The current data are consistent with the above molecular transport based hypothesis in two ways. First, the minima for the constant K_{max} occurred at a lower ΔK value (5 MPa$\sqrt{m}$) and showed a less severe dip despite a lower exposure ($6.5x10^{-3}$ Pa-s) compared to the current data at 0.027 Pa-s. This is consistent with the anticipated effect of the increased R (≈0.7-0.8 at 3-5 MPa$\sqrt{m}$) for the constant K_{max} test. Specifically, the increased crack opening associated with higher R would (a) delay the onset of roughness impeded diffusion-based flow to lower ΔK and (b) decrease the threshold exposure level for this behavior and the magnitude of the dip for a given exposure. Second, since the apparent threshold behavior is hypothesized to be due to a crack wake morphology effect it is reasonable that the K-rise data do not exhibit the strong dip observed in the K-shed data. The mechanistic cause for the plateau in the low ΔK regime of the K-rise portion of the 0.027 Pa-s data is not yet fully understood. While the current data are consistent with previous experimental work, fractography, and mechanistic interpretation the applicability of this hypothesis to the current data needs to be validated via additional microscopy, study of the closure behavior, and analysis of the roughness versus opening displacement. It is necessary to establish if this apparent threshold behavior is inherent to the material or is a crack wake effect associated with a K-shed protocol because (a) it is a scientifically novel and rich topic, and (b) the former would be incorporated into a life prediction protocol, however the latter would require modification of the data collection methods to eliminate this behavior.

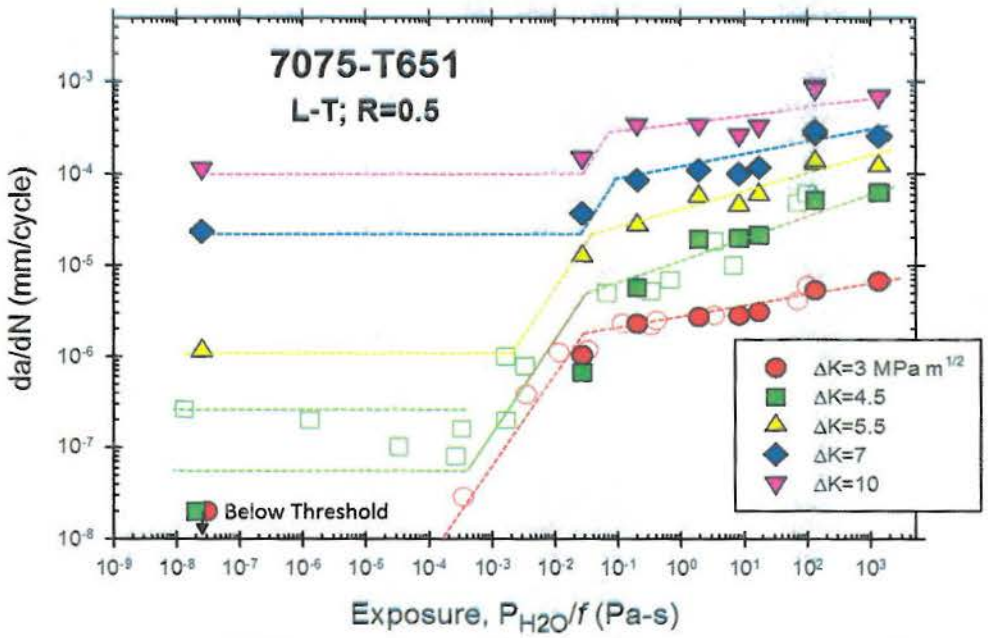

Figure 3: Fatigue crack growth rates (Figure 2) vs. exposure parameter for 7075-T651 (filled symbols), also included are prior data obtained at *R*=0.5, *f*=20 Hz and constant *ΔK* segments at various exposures (open symbols) [3,4].

Growth rates taken from Figure 2 are plotted versus exposure at constant *ΔK* in Figure 3 (filled symbols), along with growth rates for this lot of material previously generated at several levels of constant applied *ΔK* and *R*=0.5, with segments of variable exposure at a single frequency of 20 Hz (open) [3,4]. Trend lines are included to capture trends in the data and reflect theoretically based models [20,26]. These data illustrate three distinct regimes typical of such exposure plots. Specifically, (1) at low exposures there is unsufficient water vapor to enable HEE so the crack growth is governed fully by mechanical damage accumulation and independent of P_{H2O}/f, (2) crack growth is limited by molecular transport to the crack tip, in instances where such transport is governed by Knudsen flow this *da/dN* is directly proportional to P_{H2O}/f, and (3) at higher exposures there is a mild dependence on P_{H2O}/f which is controversially attributed a change in the rate limiting process to H diffusion within the process zone [20,21,26]. These data illustrate a large (three order of magnitude) increase in *da/dN* with increasing exposure level from UHV to 1334 Pa-s at low *ΔK* (3 and 4.5 MPa√m). While still significant, this increase incrementally decreases in magnitude as the *ΔK* rises to 10 MPa√m where there is a 10-fold increase in *da/dN*. This is mainly due to a large increase in the low exposure levels at higher *ΔK*, which is consistent with a larger contribution of purely mechanical damage accumulation. Comparison of current results with data from constant *ΔK* segments (open) show excellent agreement at both 3 and 4.5 MPa√m, with the only outlier being 0.027 Pa-s at 4.5 MPa√m which is within the threshold transition region in Figure 2. This outlier is expected since the dip is hypothesized to be caused by crack wake impeded flow that is not present in the constant *ΔK* segment testing. Furthermore the direct relationship between *da/dN* and P_{H2O}/f is based on the assumption of Knudsen flow controlled molecular transport, these models include empirical constant α and β related to surface

roughness and flow. As such direct comparison of values is only rigorous for constant values of surface roughness and flow properties (i.e. α and β) which is not realized for the outlying data point.

2199-T86 Growth Rates at Variable P_{H2O}/f

Fatigue crack growth rates are shown in Figure 4 for AA 2199-T86 as a function of ΔK and the exposure parameter P_{H2O}/f. Similar to the AA 7075-T651 data, there is no frequency dependence seen between 95% RH tests at 2 and 20 Hz. Above 9 MPa√m decreasing exposure from 133 to UHV shows a systematic decrease in fatigue crack growth rate; similar decreases are also observed below 5 MPa√m prior to threshold. The threshold values show a strong environmental dependence; no threshold is observed for the 1334-17 Pa-s (down to 2 MPa√m) and values of 2.3, 2.7, and 5 MPa√m are observed for 8.25, 1.9, and 0.027/UHV, respectively. The correspondence between the 0.027 Pa-s and UHV data demonstrate the elimination of environmental influences at higher exposures than observed for the AA 7075-T651. The 0.2 Pa-s, and to a lesser extent the 1.9 Pa-s, show more significant decreases in growth rate between 9 and 5 MPa√m. The apparent threshold, minima, and subsequent increase observed at 0.2 Pa-s is akin to the threshold transition behavior observed in the AA 7075-T651. However, testing of peak-aged AA 2090 (L-T) suggests that the expected fracture morphology is different and more complex for the AA 2199 compared to AA 7075-T651. Specifically, in AA 2090 SBC was found in inert environments at all ΔK, whereas in humid (H-producing) environments relatively flat crystallographic {100} cracking is expected below ≈3 MPa√m transitioning to a combination of SBC and sub-boundary cracking (which is flat) at higher ΔK [31]. Microscopy of the fracture surface and closure analysis are necessary to establish the true fracture surface morphology and to determine if the observed behavior is governed by a mechanism similar to that proposed for the AA 7075 or if other extrinsic toughening or environmental mechanisms govern this behavior.

Growth rates from Figure 4 are plotted versus exposure at constant ΔK in Figure 5 (filled symbols), along with the trend (black line) from a separate lot of 2199-T86 at 7 MPa√m, R=0.58, and f = 20 Hz where segments of various exposures were tested on a single sample [1]. Data at 3 and 4.5 MPa√m reflect cracking below the threshold at UHV and 0.27 Pa-s, and the remainder of the data fall within the diffusion controlled regime. The data show a ≈25-, 20-, and 8-fold increase in growth rates going from UHV to 1334 Pa-s at 5.5, 7 and 10 MPa√m; this trend is consistent with the increased role of mechanical damage. The magnitude of these increases are similar to that observed in AA 7075 (but slightly lower at 5.5 MPa√m). The current data aligns well with prior constant ΔK variable exposure data (black line), particularly at low and high exposures. The lack of alignment at 1.9 and 0.2 Pa-s suggests that the dip in growth rate observed between 9 and 5 MPa√m in Figure 4 is due to a crack surface morphology history effect. Similar constant ΔK variable exposure tests are justified to further investigate the mechanicstic process that governs the dip observed in Figure 4 and to inform if and how such behavior is incorporated into fracture mechanics based life predictions.

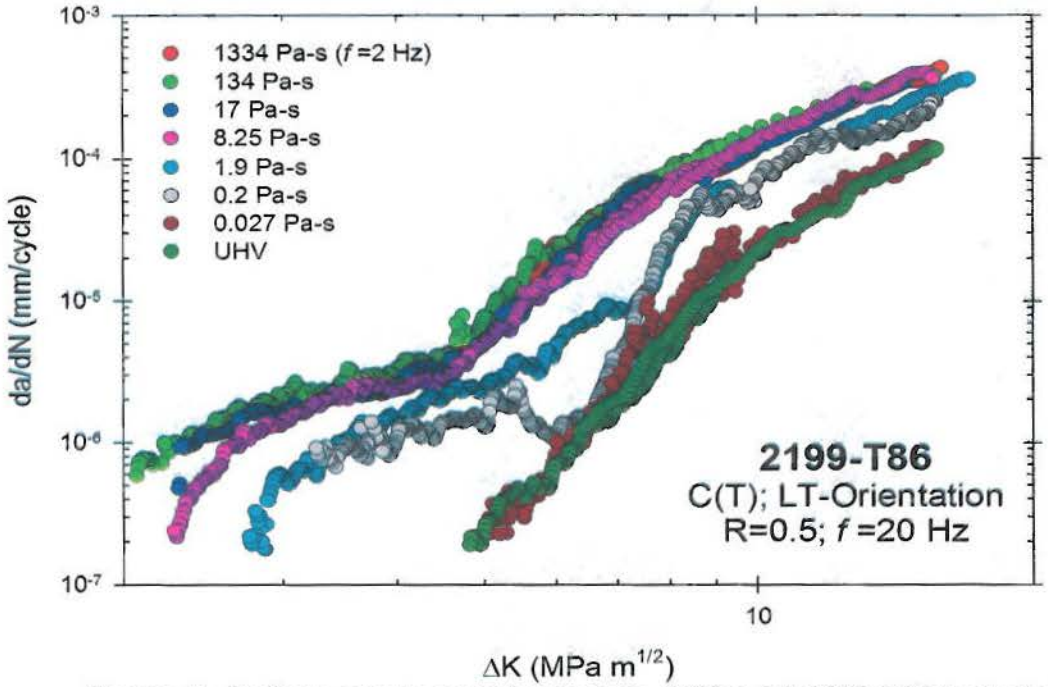

Figure 4: Fatigue crack growth rates vs. ΔK for AA 2199-T86 tested at R=0.5 in a K-shed and K-rise protocol at various levels of environmental exposure.

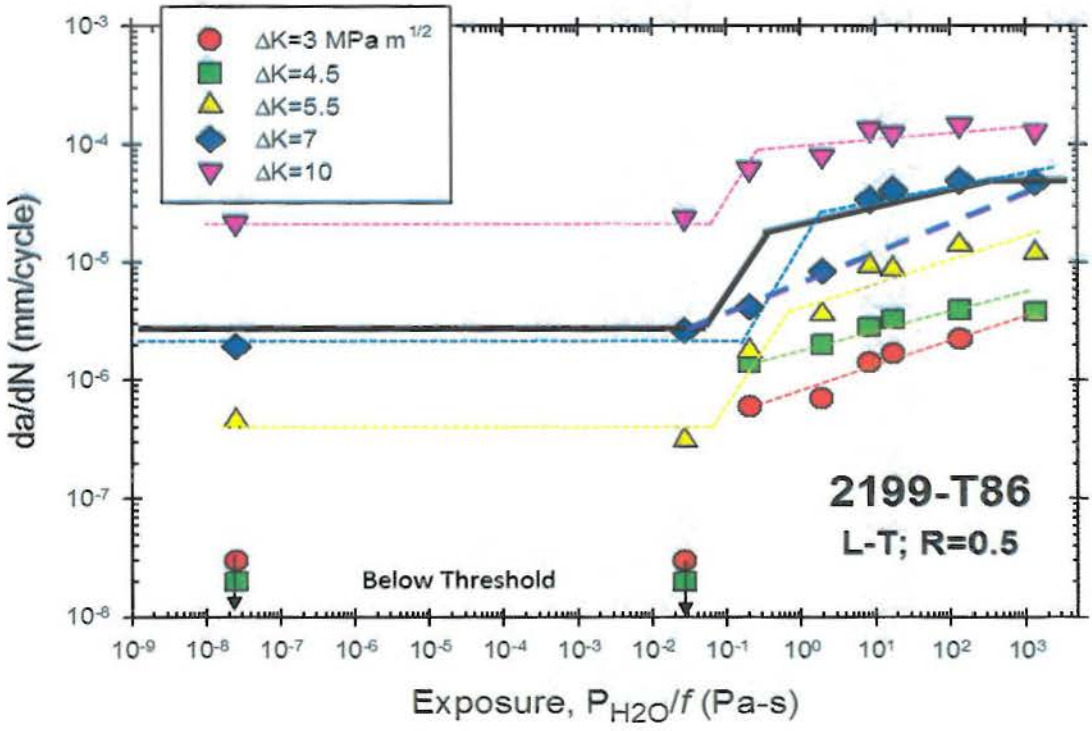

Figure 5: Fatigue crack growth rates (Figure 4) vs. exposure parameter for AA 2199-T86, also included are prior data obtained at ΔK=7 MPa$\sqrt{m}$, R=0.58, and f=20 Hz at various exposures (solid black line) [1]. The purple dashed line represents a direct interpolation approach detailed in the text.

Relevance to Prognosis

The data presented in Figure 2 and Figure 4 demonstrate that there can be a significant reduction in crack growth rate associated with P_{H2O} values that are relevant to airframe environments. These material property data are a necessary input for a fracture mechanics based model to achieve life predictions that reflect changes in loading environment. An algorithm could easily be incorporated into a software-based life prediction tool to select a growth rate that is specific to a coupled environment (i.e. P_{H2O}/f) and loading condition (ΔK); this growth rate would then be used in the iterative integration protocols that are currently employed. However, this work highlights two issues with such an approach: data fidelity that is not compromised by testing protocol-specific effects and experimental burden. First, preliminary analysis detailed above suggests that the threshold transition behavior observed in both AA 2199 and AA 7075 is governed by impeded/enhanced molecular flow that may be specific to the loading protocol or testing configuration. While the effect of fracture morphology on the H-embrittlement process is real and scientifically important, this behavior will vary with crack geometry, loading ratio, ΔK, and environmental exposure; as such these beneficial effects should not be included in growth rates for prognosis until they are fully understood and can be systematically incorporated. This approach will ensure the conservatism of the life prediction models. Further study is necessary to conclusively determine the governing mechanisms for the threshold transition behavior, however current data suggest that a K-rise loading protocol may preclude this behavior. Second, despite the potential to significantly increase the fidelity of life predictions methods and extend inspections intervals, the significant experiment burden associated with generating the data in Figure 2 and 4 is a barrier to acceptance in the structural integrity community.

A simplistic approach to reducing the experimental burden would be gathering full *da/dN*-ΔK data at a P_{H2O} commensurate with the lowest expected temperature (e.g. 0.54 Pa at -65°C) and at high humidity then linearly interpolating at the ΔK of interest between these two data sets to get a growth rate associated with the exposure of interest. Such an approach would be successful if the lowest exposure is within the diffusion controlled regime (e.g. Figure 3; 5.5 MPa$\sqrt{m}$) or if molecular flow regime spans a small range of *da/dN* (e.g. Figure 3; 10 MPa$\sqrt{m}$). However, if these conditions are not meet then this approach would yield unconservative *da/dN* values as demonstrated by the purple-dashed line in Figure 5 for AA 2199-T86 at 7 MPa$\sqrt{m}$. An alternate approach would be to leverage limited full *da/dN*-ΔK data-sets with testing at isolated constant ΔK values and various exposure level segments (as presented in Figure 3 and 5) where ≈20-30 data points can be efficiently gathered on a single specimen. In this paradigm the high humidity and UHV testing would set the baseline bounding conditions over the entire ΔK range (and R) of interest. The constant ΔK variable exposure segment data would be used to generate trend lines that are consistent with the governing theories (i.e. direct proportionality in the Knudsen flow regime) as shown in Figure 3, 5 and 6. These lines or linear interpolation between these lines (for ΔK not tested) would be used to determine the reduction in growth rate associated with a given exposure below the high humidity level. For example, to determine the AA 7075-T651 growth rates associated with 10 Pa-s and ΔK of 4 MPa$\sqrt{m}$, first you would linearly interpolate between the 3.5 and 4.5 MPa$\sqrt{m}$ trend lines at both high humidity and 10 Pa-s to get values at 4 MPa$\sqrt{m}$ (stars in Figure 6). These values would be used to establish a percent reduction in growth rate below the high humidity level. Next the full high humidity *da/dN*-ΔK relationship would be used to obtain the baseline humid *da/dN* value, which would be multiplied by the percentage calculated in the previous step to give the desired *da/dN* for a ΔK of 4 MPa$\sqrt{m}$ and 10 Pa-s. For low ΔK and exposure values the threshold may not be exceeded, as such a conservative approach would be to use the low exposure trend line from the higher stress level. Details such as what constant ΔK values to probe, the

details of the trend line interpolation, the R-ratio of interest, and testing protocol to obtain the full da/dN-ΔK relationships can be customized based on the needs of the application. This strawman demonstrates an approach that could be reasonably incorporated into a LEFM prediction code with a non-prohibitive experimental burden for developing the material properties.

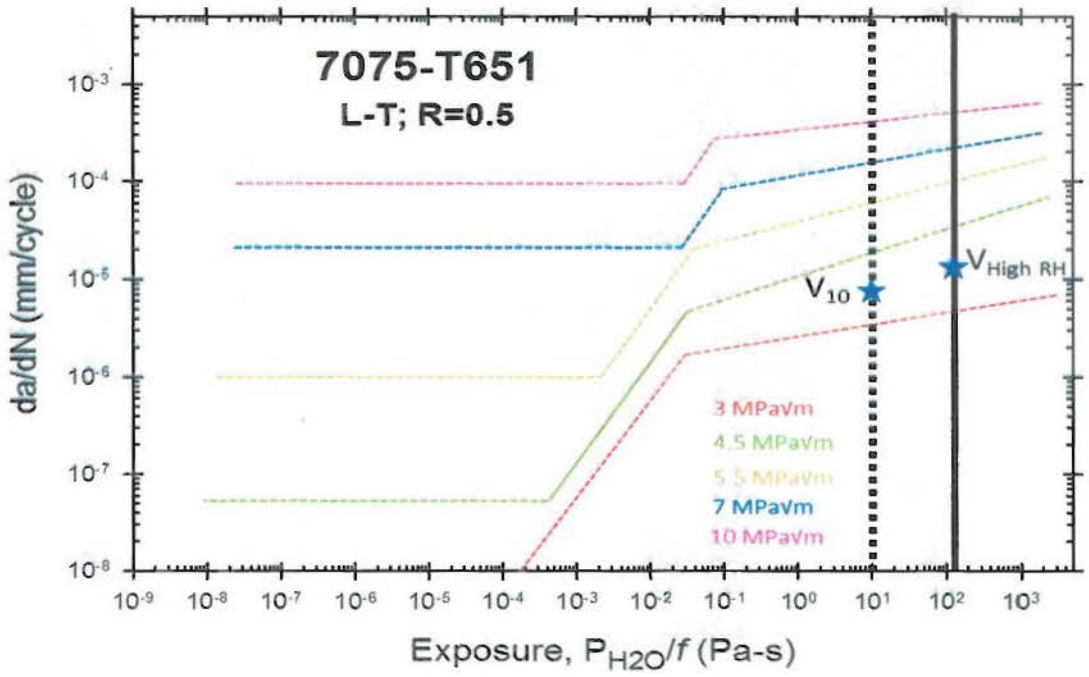

Figure 6: Fatigue crack growth rate trends vs. exposure parameter for AA 7075-T651. A process for calculating the ΔK and exposure specific *da/dN* is schematically outlined consistent with the scenario described in the text.

Future Work

The experimental data presented in Figures 1-5 quantifies the effect of various water vapor environments on the crack growth rate over a wide range of ΔK, including the threshold regime, enabling analysis in the context of both prominent H-embrittlement models and LEFM life prediction methodologies. However, continued data analysis is required to better understand the observed behavior. Specifically, microscopy is necessary to establish the crack morphology associated with the changes in the growth rates; this information will enable evaluation of the presented hypotheses which are based on prior fracture surface characterizations. Furthermore, analysis of the adjusted compliance ratio and ASTM 2% closure values calculated based on the crack tip opening displacement measurements can be coupled with characterization of the fracture surface roughness to provide a better understanding of the level of closure and convective mixing and how each influence crack growth kinetics. Additional testing will also be performed to (a) evaluate the efficacy of the P_{H2O}/f parameter when the frequency is the independent variable rather than the water vapor pressure, (b) further evaluate the threshold transition behavior by testing AA 7075 at 0.09 and 0.009 Pa-s and 2199 at 0.9 and 0.09, and (c) to independently establish the trendlines seen in Figures 3, 5 and 6 by testing at constant ΔK and various expsoure values.

While the testing and analysis above will provide further insights into the processes and mechanisms that govern the fatigue behavior, continued research is also necessary to inform the incorporation of the flight environment into a fracture mechanics methodology. Specifically, understanding how the environmental effects *R*-interpolation rules (Forman, Harter T, etc.), understanding transient effects during environment changes, developing the software algorithm to incorporate the strawman approach detailed above, detailing a coupled load-environment spectrum that reflects true airframe component conditions, and further evaluation of temperature dependencies to understand the conservative error associated with using P_{H2O} as a proxy for low temperature environments. The strong influence of high altitude environments demonstrated in this and companion work justifies such efforts to inform rigorous assumptions for a LEFM approach that are supported by scientific understanding [6,12,37].

CONCLUSIONS

Compliance-based characterization of CT specimens fatigued under *K*-shed and *K*-rise loading protocols at high *R* (0.5) and water vapor pressures applicable to airframe operation yielded a novel set of fatigue crack growth rates that extended to the threshold regime for two aerospace Al alloys (7075-T651 and 2199-T86). These data were analyzed with respect to prominent environmental fatigue theories and used to inform a next generation prognosis approach that increases rigor and accuracy by incorporating the effects of loading environment. The following conclusions are established:

- The Al-Cu-Li alloy 2199-T86 exhibited enhanced fatigue crack growth rate resistance compared with 7075-T651 over a wide range of environmental exposures and ΔK, consistent with literature expectations.
- The wide range da/dN-ΔK data for AA 7075-T651 and AA 2199-T86 shows the expected decrease in growth rate with decreasing exposure parameter of P_{H2O}/f. Plots of crack growth rate versus exposure parameter show that current data reasonably conform to prominent environmental theories where the crack growth is limited by either molecular flow or H-diffusion in the crack tip process zone.
- Threshold transition behavior was observed in both AA 7075-T651 and AA 2199-T86 , where *K*-shed data show an apparent threshold followed by an increase in growth rates with falling ΔK. Speculatively, this is due to development of crack wake roughness that initially impeeds molecular flow; subsequent increasing roughness then causes convective mixing which enhances flow and increases growth rates.
- A strawman approach to selecting environment appropriate crack growth rates for LEFM modeling protocol is put forth that is justified by experimental data, incorporates mechanism based assumptions, and limits the experimental burden associated with developing the crack growth rate database.

ACKNOWLEDGEMENTS

This material is based on research sponsored by the US Air Force Academy under agreement number FA7000-11-2-0011. This work is performed in collaboration with Dr. Jennifer Warner-Locke at the ALCOA Technical Center. The U.S. Government is authorized to reproduce and distribute reprints for Governmental purposes notwithstanding any copyright notation thereon.

The views and conclusions contained herein are those of the authors and should not be interpreted as necessarily representing the official polices and endorsements, either expressed or implied of US Air Force Academy or the US Government. Approved for public release, distribution is unlimited.

REFERENCES

1. Ro YJ, Agnew SR, Bray GH, Gangloff RP (2007) Environment-exposure-dependent fatigue crack growth kinetics for Al-Cu-Mg/Li. *Materials Science and Engineering A*. **468**: 88-97.
2. Ranganathan N, McKeighan PC (2005) *Fatigue testing and analysis under variable amplitude loading conditions, STP 1439*. ASTM International, West Conshohocken, PA.
3. Bush RW, Ai JH (2010) Unpublished research. University of Virginia, Charlottesville, VA.
4. Papazian J, Anagnostou EL, Christ RJ, et al. (2009) DARPA/NCG structural integrity prognosis system, HR0011-04-C-0003. DARPA, Arlington, VA.
5. Potter JM, Watanabe RT (1989) *Development of Fatigue Loading Spectra, STP 1006*. ASTM International, West Conshohocken, PA.
6. Burns JT, Gangloff RP, Bush RW (2011) Effect of environment on corrosion induced fatigue crack formation and early propagation in aluminum alloy 7075-T651. *DoD NACE Corrosion Conference*, Palm Springs, CA.
7. Schutz D, Gerharz JJ (1987) ENSTAFF--a standard test sequence for composite components cominging load and environment. In: Simpson DL, ed. *New Materials and Fatigue Resistant Aircraft Design*. ICAF 14, Ottawa, Ont, 425-444.
8. de Jonge JB, Spiekhout DJ (1979) Use of AIDS recorded data for assessing service load experience. In: Abelkis PR, Potter JM, eds. *Service Fatigue Loads Monitoring, Simulation, and Analysis, ASTM STP 671*. ASTM International, West Conshohocken, PA, 48-66.
9. Wanhill RJH (2001) Flight simulation fatigue crack growth guidelines, NRL-TP-2001-545. NRL, Amsterdam, The Netherlands.
10. Wiederhold PR (1997) *Water Vapor Measurement Methods and Instrumentation*. CRC Press, New York, NY.
11. Atmosphere USCoEttS (1976) *U.S. standard atmosphere, 1976*. National Oceanic and Amospheric Administration, Washington, D.C.
12. Burns JT, Gangloff RP (2012) Effect of loading environment on fatigue crack formation and microstructurally small fatigue propagation in Al-Zn-Mg-Cu. *Metall Mater Trans A*. In Press; DOI: 10.1007/s11661-11012-11374-11663.
13. Hochhalter JD, Littlewood DJ, Veilleux MG, et al. (2011) A geometric approach to modeling microstructurally small fatigue crack formation: III. Development of a semi-empirical model for nucleation. *Model Simul Mater Sc*. **19**.
14. Manonukul A, Dunne FPE (2004) High- and low-cycle fatigue crack initiation using polycrystal plasticity. *P Roy Soc Lond a Mat*. **460**: 1881-1903.
15. McDowell DL, Dunne FPE (2010) Microstructure-sensitive computational modeling of fatigue crack formation. *Int J Fatigue*. **32**: 1521-1542.
16. Robertson IM (2001) The effect of hydrogen on dislocation dynamics. *Eng Fract Mech*. **68**: 671-692.
17. Robertson IM, Martin ML, Fenske JA (2011) Modeling damage mechanisms in hydrogen embrittlement. In: Gangloff RP, Somerday BP, eds. *Gaseous hydrogen embrittlement of materials in energy technologies*. Woodhead Publishing Limited, Cambridge, UK.

18. Oriani RA (1987) Whitney Award Lecture 1987 - Hydrogen - the versatile embrittler. *Corrosion*. **43**: 390-397.
19. Ro Y, Agnew SR, Gangloff RP (2008) Environmental fatigue-crack surface crystallography for Al-Zn-Cu-Mg-Mn/Zr. *Metall Mater Trans A*. **39A**: 1449-1465.
20. Wei RP, Gao M (1990) Hydrogen embrittlement and environmentally asisted crack growth. In: Moody NR, Thompson AW, eds. *Hydrogen Effects on Material Behavior*. TMS-AIME, Warrendale, PA, 789-813.
21. Ruiz J, Elices M (1997) Effect of water vapour pressure and frequency on fatigue behaviour in 7017-T651 aluminium alloy plate. *Acta Mater*. **45**: 281-293.
22. Wei RP, Pao PS, Hart RG, Weir TW, Simmons GW (1980) Fracture-mechanics and surface-chemistry studies of fatigue crack-growth in an aluminum-alloy. *Metall Trans A*. **11**: 151-158.
23. Pao PS, Gao M, Wei RP (1988) Critical assessment of the model for transport-controlled fatigue crack growth. In: Wei RP, Gangloff RP, eds. *Basic Questions in Fatigue, ASTM STP 924*. ASTM International, West Conshohocken, PA, 182-195.
24. Gao M, Pao PS, Wei RP (1988) Chemical and metallurgical aspects of environmentally assisted fatigue crack-growth in 7075-T651 aluminum-alloy. *Metall Trans A*. **19**: 1739-1750.
25. Weir TW, Simmons GW, Hart RG, Wei RP (1980) Model for surface-reaction and transport controlled fatigue crack-growth. *Scripta Metall Mater*. **14**: 357-364.
26. Gasem ZM, Gangloff RP (2001) Rate-limiting processes in environmental fatigue crack propagation in 7000-series aluminum alloys. In: Jones RH, ed. *Chemistry and electrochemistry of corrosion and stress corrosion cracking: A symposium honoring the contributions of RW Staehle*. TMS-AIME, Warrendale, PA, 501-521.
27. Piascik RS, Gangloff RP (1991) Environmental fatigue of an Al-Li-Cu alloy 1. Intrinsic crack-propagation kinetics in hydrogenous environments. *Metall Trans A*. **22**: 2415-2428.
28. Giummarra C, Rioja RJ, Bray GH, Magnusen PE, Moran JP (2008) Al-Li Alloys: Development of corrosion resistant, high toughness, aluminum-lithium aerospace alloys. In: Hirsh J, Skrotzki B, Gottstein G, eds. *Aluminum Alloys: Their Physical and Mechanical Properties*. Wiley-VCH, Weinheim, Germany.
29. Rao KTV, Yu W, Ritchie RO (1988) Fatigue Crack-Propagation in Aluminum-Lithium Alloy 2090 .2. Small Crack Behavior. *Metall Trans A*. **19**: 563-569.
30. Rao KTV, Yu W, Ritchie RO (1988) Fatigue Crack-Propagation in Aluminum-Lithium Alloy 2090 .1. Long Crack Behavior. *Metall Trans A*. **19**: 549-561.
31. Piascik RS, Gangloff RP (1993) Environmental fatigue of an Al-Li-Cu alloy. Part 2: Microscopic hydrogen cracking processes. *Metall Trans A*. **24**: 2751-2762.
32. Gupta VK, Agnew SR (2011) Fatigue crack surface crystallography near crack initiating particle clusters in precipitation hardened legacy and modern Al-Zn-Mg-Cu alloys. *Int J Fatigue*. **33**: 1159-1174.
33. Shih TH, Wei RP (1983) The Effects of Load Ratio on Environmentally Assisted Fatigue Crack-Growth. *Eng Fract Mech*. **18**: 827-837.
34. Hartt WH, Martin PE, Hooper WC (1979) Endurance limit enhancement of structural steel in sea water by cathodic protection. *Offshore Technology Conference*, Houston, TX.
35. Turnbull A (1982) A Theoretical Evaluation of the Influence of Mechanical Variables on the Concentration of Oxygen in a Corrosion Fatigue Crack. *Corros Sci*. **22**: 877-893.
36. Turnbull A, Ferriss DH (1987) Mathematical-Modeling of the Electrochemistry in Corrosion Fatigue Cracks in Steel Corroding in Marine Environments. *Corros Sci*. **27**: 1323-1350.
37. Burns JT, Gangloff RP (2011) Scientific advances enabling next generation management of corrosion induced fatigue. *Procedia Engineering*. **10**: 362-369.